NUMERICAL ANALYSIS OF ULTRASONIC VIBRATION ENHANCED FRICTION STIR WELDING OF DISSIMILAR AL/MG ALLOYS

C. L. YANG*,**, C. S. WU*, M. BACHMANN**,
M. RETHMEIER***,**,****

**Institute of Materials Joining, Shandong University, Jinan 250061, China*
***Welding Technology, Bundesanstalt für Materialforschung u. -prüfung (BAM), Unter den Eichen 87, 12205 Berlin, Germany*
****Institute of Machine Tools & Factory Management, Technische Universität Berlin, Pascalstraße 8-9, 10587 Berlin, Germany*
*****Joining and Coating Technology, Fraunhofer Institute for Production Systems and Design Technology, Pascalstraße 8-9, 10587 Berlin, Germany*

DOI 10.3217/978-3-85125-968-1-29

ABSTRACT

The ultrasonic vibration enhanced friction stir welding (UVeFSW) process has unique advantages in joining dissimilar Al/Mg alloys. While there are complex coupling mechanisms of multi-fields in the process, it is of great significance to model this process, to reveal the influence mechanism of ultrasonic vibration on the formation of Al/Mg joints.

In this study, the acoustic-plastic constitutive equation was established by considering the influence of both ultrasonic softening and residual hardening on the flow stress at different temperatures and strain rates. And the ultrasonic induced friction reduction (UiFR) effect on friction coefficient in different relative directions at the FSW tool-workpiece interface was quantitatively calculated and analyzed.

The Al/Mg UVeFSW process model was developed by introducing the above acoustic effects into the model of Al/Mg friction stir welding (FSW). The ultrasonic energy is stronger on the aluminum alloy side. In the stirred zone, there is the pattern distribution of ultrasonic sound pressure and energy. The heat generation at the tool-workpiece contact interface and viscous dissipation were reduced after applying ultrasonic vibration. Due to the UiFR effect, the projections of friction coefficient and heat flux distributions at the tool-workpiece interface present a "deformed" butterfly shape. The calculated results show that ultrasonic vibration enhanced the material flow and promoted the mixing of dissimilar materials.

Keywords: Friction stir welding; Ultrasonic vibration; Al/Mg alloys; Numerical simulation

INTRODUCTION

With the development of the economy and society, the demand for energy conservation and emission reduction has increased, and light materials such as aluminum and magnesium alloys are widely used in automobile, aerospace, and high-speed train industries [1]. This inevitably faces welding of dissimilar Al/Mg alloys, and the joining of aluminum alloy and magnesium alloy can make full use of their advantages and make up

for each other's shortcomings. However, due to the great differences in crystal structure and physical properties between the two materials, the high-quality joining of Al/Mg dissimilar alloys faces special challenges [2]. Although friction stir welding (FSW) has some prominent advantages in the joining of Al/Mg alloys [2-5], there is still growing demand for further improvement in the microstructures and mechanical properties of dissimilar joints.

Recently, ultrasonic vibration has been used to improve the FSW process of dissimilar material FSW. Sachin et al. [6] applied ultrasonic vibration to the tool along the welding direction. Strass et al. [7-10] exerted the ultrasonic vibration to one side of the workpiece through rollers. Ji et al. [11-13] conducted the static shoulder FSW with the ultrasound applied to the back of the workpieces. Lv et al. [14] used the ultrasonic vibration enhanced FSW (UVeFSW) for joining Al/Mg alloys, and the ultrasonic vibration was applied to the top surface of the workpieces in front of the tool. All the above experimental studies show that ultrasonic vibration can improve weld quality and decrease welding loads.

However, there are complex coupling mechanisms of multi-fields in the Al/Mg dissimilar UVeFSW process, and the influence of ultrasonic vibration on the "heat generation/temperature profile-stress/strain-material flow-material mixing" behaviors is more complex. Therefore, it is of great significance to model the UVeFSW process of dissimilar Al/Mg alloys and conduct the coupled numerical analysis of multi-physical fields, to reveal the influence mechanism of ultrasonic vibration on the formation of dissimilar Al/Mg joints and realize the effective utilization of ultrasonic energy field in friction stir welding of dissimilar Al/Mg alloys.

For dissimilar FSW of Al/Mg alloys without ultrasonic assistance, Singh et al. [15] established a heat transfer model of 6061 Al/AZ31 Mg, and Lim et al. [16] developed a finite element model based on the coupled Euler-Lagrange method for Al 6061-T6 and AZ61 Mg to predict the temperature and strain. The authors' group has established computational fluid dynamics (CFD) model of Al-Mg considering local turbulence [17]. On the other hand, for the UVeFSW of a single material (Al alloy), Shi et al. established a CFD model which considered the acoustic softening effect [18], on this basis, the acoustic softening & residual hardening effects [19] and the ultrasonic induced friction reduction (UiFR) effect were considered [20] separately. However, the ultrasonic field induces all these influences simultaneously during the UVeFSW process of Al/Mg alloys, which should be considered in a single comprehensive model.

In this study, a multi-physical coupling model including the acoustic plasticity (softening & residual hardening effects) and UiFR effect was developed and experimentally validated for UVeFSW of dissimilar Al/Mg alloys. The ultrasonic effects on the friction coefficient, heat generation, temperature, and material flow fields were analyzed quantitatively.

EXPERIMENT

In the Al-Mg UVeFSW process, as shown in Fig. 1, ultrasonic vibration is transmitted to the top of the workpiece in front of the FSW tool directly through the sonotrode at a certain angle. FSW was performed on dissimilar AZ31B-H24 Mg and 6061-T4 Al alloys.

The Mg alloy sheet was on the advancing side (AS), and the Al alloy sheet was on the retreating side (RS). The sheet size was 200 mm (length) × 60 mm (width) × 3 mm (thickness). The FSW tool constituted a concave shoulder (diameter 12 mm) and a frustum-shaped right-hand threaded pin (tip diameter 4.2 mm, root diameter 3.2 mm, and length ground from 3 mm to 2.7 mm), and its material was tool steel. The tool was rotated anticlockwise with a tilt angle of 2.5°. The tool rotation speed, welding speed, and shoulder plunge depth were 800 rpm, 50 mm/min, and 0.15 mm respectively. The tool offset was 0.3 mm to the Mg sheet (AS). The frequency of the ultrasonic vibration is 20 kHz, the amplitude is 40 μm, and the effective power is 220 W. The radius of the sonotrode tip is 4.0 mm, the center of the tip is 20 mm away from the axis of the FSW tool, and the angle between the axis of the sonotrode with the welding direction is 40 °, the pressing force on the sonotrode is 300 N.

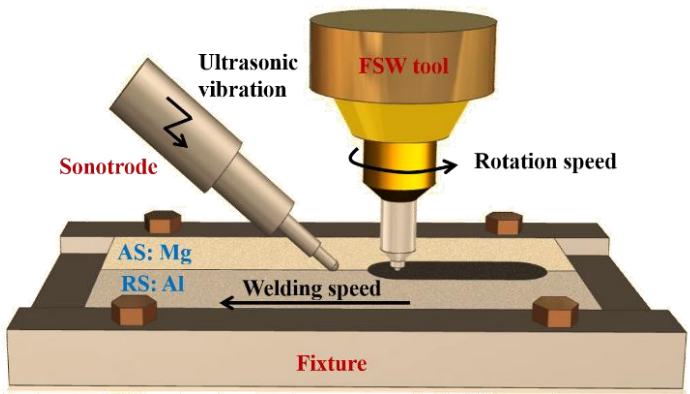

Fig. 1 Schematic of Al-Mg UVeFSW

After welding, metallographic samples at the horizontal section around the keyhole for FSW and UVeFSW were prepared.

AL/MG UVEFSW CFD MODEL

The Al/Mg dissimilar UVeFSW model is a combination of the UVeFSW model with acoustic softening and hardening effects [19], the UVeFSW model considering the UiFR effect [20], and the Al/Mg dissimilar FSW model [17]. The geometric model of the Al/Mg UVeFSW process is shown in Fig. 2.

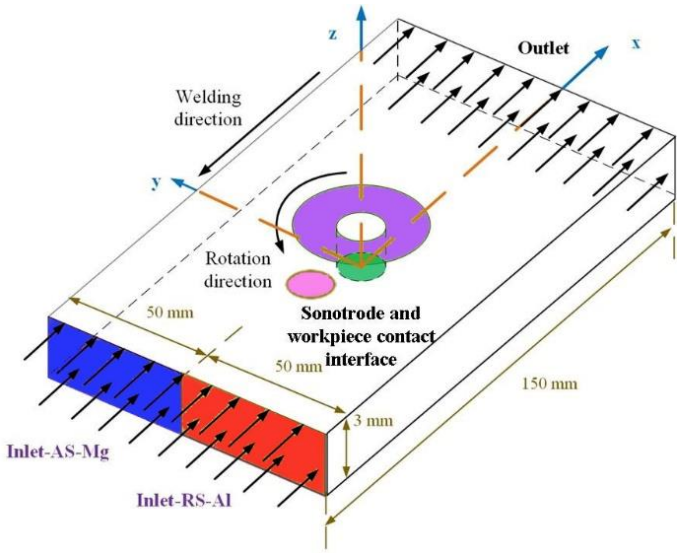

Fig. 2 The geometry model in UVeFSW of Al/Mg alloys

There are three kinds of acoustic effects considered during the welding process model: the preheat effect, the acoustic-plastic effect (acoustic softening and residual hardening effects) as well as the ultrasonic induced friction reduction (UiFR) effect.

THE PREHEAT EFFECT

When the ultrasound is applied, not only frictional heat is generated on the sonotrode-workpiece interface, but also the heat due to plastic deformation exists.

According to the frictional law, the heat generated (Q_F) at the interface between the ultra-sonic horn and the workpiece is as follows [21],

$$Q_F = \frac{4\xi_0 f_W \cos\varpi \mu_{\text{tool}} F_N}{A_{\text{tool}}} \tag{1}$$

where ξ_0 is the amplitude of the ultrasonic vibration, f_W is the frequency of the ultrasonic vibration, ϖ is the angle between the sonotrode and the workpiece surface (horizontal plane), F_N is the axial pressure due to the clamping force acting on the sonotrode, μ_{tool} is the friction coefficient at the sonotrode-workpiece contact interface, and A_{tool} is the area of sonotrode–workpiece contact interface.

The heat (Q_W) generated by plastic deformation at the contact surface between the ultrasonic horn and the workpiece can be expressed by the following equation,

$$Q_W = \sqrt{\left(\frac{\sigma_y}{2}\right)^2 - \left(\frac{F_N / A_{\text{tool}}}{2}\right)^2}\, 4\xi_0 f_W \cos\varpi \tag{2}$$

where σ_y is the temperature-dependent yield stress.

The total heat generation at the sonotrode-workpiece contact interface is written as,

$$Q_{s-w} = Q_F + Q_W \tag{3}$$

THE ACOUSTIC PLASTIC EFFECT

In the upsetting process of metal samples, when ultrasonic is applied at a certain moment, the stress decreases, which indicates that the deformation resistance of the material decreases due to ultrasonic action, which is called the acoustic softening effect. If the ultrasonic action time is long enough, the stress will increase when the ultrasonic application is stopped, which is called the acoustic residual hardening effect [22].

In the process of applying ultrasound, the dislocations in the material absorb acoustic energy, so that they are easier to be activated and leave their pinned equilibrium positions, and the amplitude of dislocation oscillation increases until they exceed the normal distance from the equilibrium positions. As the dislocation absorbs additional acoustic energy, the shear stress required for metal plastic deformation is significantly reduced, which is called the acoustic softening effect.

When there is a superposition of acoustic stress and internal stress caused by lattice defects, dislocations are forced to move in the preferred direction, thus changing the internal structure. In other words, the material properties will change permanently, and the ultrasound enhances the proliferation and redistribution of dislocations, which will lead to the acoustic hardening effect.

During the process of ultrasonic application, the activated dislocations are much larger than the proliferated dislocations, and finally, show a softening effect. However, when the application of ultrasound is stopped, the activation disappears, but the dislocation proliferation caused by the application of ultrasound is permanent, so it shows the hardening effect.

Although we calculate the situation in the process of ultrasonic application, there is a difference between the final softening shown and the actual softening effect, so it is necessary to comprehensively consider the acoustic softening and hardening effects to describe the acoustic plastic effect.

In the process of metal plastic deformation, dislocations proliferate and annihilate simultaneously. The strength of dislocation proliferation and annihilation determines the increase or decrease of the dislocation density. The change of the dislocation density, in turn, determines the increase or decrease of the strength of the materials [23]. We describe the acoustic softening effect by considering the influence of ultrasonic vibration on the activation process of dislocation, and reflect the acoustic residual hardening effect by expressing the influence of ultrasound on the proliferation process of dislocation. Finally, we can use Eq. (4) to express the acoustic plastic effect of ultrasound.

What's more, for the Mg alloy AZ31B, Dong et al [24] found that the stress gradually de-creases with the increase of strain when strain is over 0.2, which is due to the softening caused by recrystallization. When the softening reaches a certain level, the stress-strain curve tends to be a straight line. On the other hand, the parameters of the constitutive equation taken by Yu et al. [25] in modeling the FSW of the magnesium alloy were all measured near the peak of the stress-strain curve (corresponding to the strain 0.2). According to the experimental results of Liu et al. [26], the strain around the tool in the FSW process can reach 35 or even higher. Therefore, the constitutive equation is modified by multiplying a softening coefficient to avoid the calculation result caused by excessive stress from being inconsistent with the experimental ones.

$$\sigma_{\mathrm{s,am}}^{\mathrm{r}} = \frac{\xi_{\mathrm{am}}}{\alpha} \ln\left\{\left(\frac{\bar{\varepsilon}}{A}\exp\left(\frac{Q_{\mathrm{s}}}{RT}\right)\right)^{1/n} + \left[1+\left(\frac{\bar{\varepsilon}}{A}\exp\left(\frac{Q_{\mathrm{s}}}{RT}\right)\right)^{2/n}\right]^{1/2}\right\} \tag{4}$$

where $\sigma_{\mathrm{s,am}}^{\mathrm{r}}$ is the flow stress, ξ_{am} is the softening coefficient when recrystallization is considered, $\bar{\varepsilon}$ is the strain rate, R is the gas constant, T is the temperature, α, A, n are the material constants, Q_{s} is the activation energy with the acoustic plastic effects, and can be expressed as follow,

$$Q_s = Q - \frac{\beta R \Delta F}{k_B}\left(\frac{E}{\tau_0 + \mu_m ab\sqrt{\rho}}\right)^m \tag{5}$$

where Q is the activation energy without the ultrasound affected, β and m are experimentally determined parameters in the model of the change in the dimensionless stress ratio caused by the acoustic softening effect, ΔF is the change of Helmholtz free energy, k_B is Boltzmann constant, E is the sound energy density, τ_0 is the lattice resistance, μ_m is the shear elastic modulus, a is a parameter close to 1/3, b is the length of the Burgers vector and ρ is the dislocation density. Based on the Kocks-Mecking (KM) [i,ii] dislocation model as well as the acoustic hardening effect, $\sqrt{\rho}$ is then expressed by the following,

$$\sqrt{\rho} = \left[k_1\left(1+\eta_{k_1}\right) - \exp\left(\frac{-k_2 \varepsilon M}{2}\right)\right] / k_2 \tag{6}$$

where k_1 is the dislocation storage coefficient, and k_2 is the dislocation dynamic recovery coefficient ε is the strain. In this study, ε takes a value of 30 [26]. The acoustic residual hardening effect is introduced into the constitutive equation model via the parameter η_{k_1}, which is the dimensionless parameter that defines the rate of change of k_1 under the action of ultrasound. M is the Taylor factor.

Using the Logistic function to describe the S-shaped saturation phenomenon of dislocation density [29-31]

$$\eta_{k_1} = KP_0 / \left[P_0 + (K - P_0) \exp(-r_a t_v) \right] \tag{7}$$

where P_0 and K are the initial and saturation values, t_v is the duration time of the ultrasound exertion, and r_a is the growth rate of dislocation density which is mainly affected by the intensity of the ultrasonic energy field. In this study, r_a is considered to be proportional to the vibration amplitude (ξ_0), and the ratio is φ, that is $r_a = \varphi \xi_0$. The duration time of the ultrasound exertion (t_v) equals to the time during which the material flows through the FSW tool shoulder (about the time when the material undergoes the combined action area of the plastic deformation and the ultrasonic vibration).

And then the viscosity μ_s is expressed as [32],

$$\mu_s = \frac{\sigma^{\mathrm{r}}_{\mathrm{s,am}}}{3\bar{\dot{\varepsilon}}} \tag{8}$$

And then the viscosity was used for the momentum equation and the viscous dissipation source
in the energy equation.

THE ULTRASONIC INDUCED FRICTION REDUCTION EFFECT

The friction coefficient between the FSW tool/workpiece is a prerequisite for determining the heat generation and velocity boundary. When ultrasonic vibration is applied in UVeFSW, the ultrasonic induced friction reduction (UiFR), i.e., the friction reduction effect due to ultrasonic vibration, must be taken into account.

The relative direction between the vibration direction and the relative sliding direction is different, and the reasons for the reduction of friction caused by ultrasound are different. Referring to the contact plane and the sliding direction, the ultrasonic vibration can be exerted in three orthogonal directions: ① In-plane parallel, i.e., longitudinal, ② In-plane perpendicular, i.e., transverse, and ③ Out-of-plane perpendicular, i.e., normal, as shown in Fig. 3.

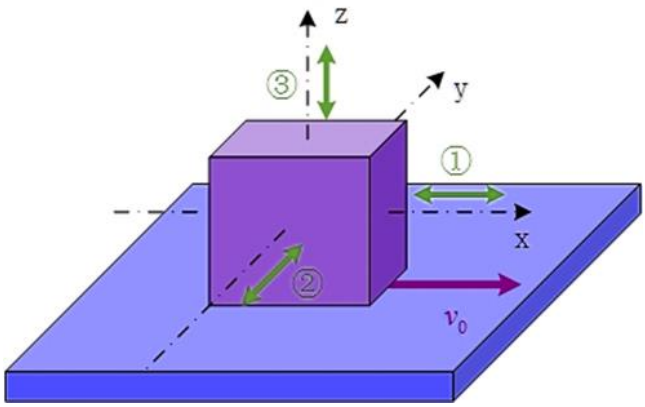

Fig. 3 Ultrasonic vibration application direction in contact friction

The ultrasonic induced friction reduction (UiFR) caused by in-plane vibration is generally interpreted as the ultrasonic reversal effect [33,34]. It implies that when the vibration occurs, the normal force and the instantaneous friction coefficient remain the same, but the direction of the friction force is changed or reversed within a vibration cycle, resulting in a decrease in the average coefficient of friction during one vibration cycle. Storck et al. proposed an ultra- sonic reversal effect model based on the Coulomb friction law [34,35]. For a slider that slides at the speed v_0, the friction coefficient without ultrasonic vibration is written as μ_0. When the ultrasonic vibration is applied along the longitudinal direction (direction ①), the amplitude of the vibration velocity is expressed by $\hat{v}$. Then, the ratio between the average friction coefficient μ_L with UiFR and the friction coefficient without UiFR in the longitudinal direction can be written as [34,35]:

$$\frac{\mu_L}{\mu_0}=\begin{cases}1 & \zeta_L \geq 1\\ \dfrac{2}{\pi}\sin^{-1}\left(\zeta_L\right) & -1<\zeta_L<1\\ -1 & \zeta_L \leq -1\end{cases} \tag{9}$$

where $\zeta_L = v_0/\hat{v}$. The subscript *L* denotes the longitudinal direction of vibration. Only if $\zeta_L = v_0/\hat{v} < 1$, i.e., $\hat{v} > v_0$, the motion direction of the slider is reversed, and the ultrasonic vibration can decrease the friction coefficient. The larger is $\hat{v}$, the more obvious the ultrasonic induced friction reduction (UiFR) is. In the UVeFSW system, the vibration amplitude at the sonotrode end is 40 μm (idle condition), and the amplitude of the vibration velocity is estimated to be 3.2 m/s. Here the amplitude of the vibration velocity ($\hat{v}$) under the idle condition is at the workpiece location with the maximum sound pressure, and the values of $\hat{v}$ at other workpiece locations are determined according to the sound pressure distribution.

When the ultrasonic vibration is applied in the transverse direction (direction ②), the

ratio of the average friction coefficient μ_T with UiFR to the coefficient of friction without UiFR in the transverse direction is written as [34,35],

$$\frac{\mu_T}{\mu_0}=\frac{2\,\mathrm{sgn}(\zeta_T)}{\pi\sqrt{1+\dfrac{1}{\zeta_L^2}}}K\left(\frac{1}{1+\zeta_L^2}\right) \tag{10}$$

where $K(s)$ is the first type of complete elliptic integral, which can be obtained by integrating the eight-node Gauss-Legendre quadrature formula.

When ultrasonic vibration is exerted in the normal direction (direction ③ in Fig. 3), the normal force of the friction pair changes periodically, which leads to the periodic change of the real interface contact area. Then, in friction metal forming under normal ultrasonic vibration, the ratio of the contact friction coefficient μ_N to the contact friction coefficient μ_0 without ultrasonic action in the normal direction is expressed as [36],

$$\frac{\mu_N}{\mu_0}=\frac{\tau-\alpha_N\xi}{\tau}\frac{H}{E^*}\cdot\sqrt{\frac{\pi R_N}{s_D}}=\left(1-\frac{\alpha_N\xi}{\tau}\right)\cdot\frac{\sqrt{\pi}}{\psi} \tag{11}$$

where τ is the shear strength without ultrasonic vibration, respectively, α_N is the relevant parameter related to the acoustic softening effect, ξ_0 is the vibration amplitude, H is the hardness of the softer material, E^* is the Hertz elastic modulus, R_N is the radius of curvature of the micro-convex peaks at the contact surface, and s_D is the standard deviation of the height of the micro-convex peaks at the contact surface, and $\psi=\left(E^*/H\right)\cdot\sqrt{s_D/R_N}$ is the plasticity index proposed by Greenwood and Williamson [36].

In UVeFSW, the ultrasonic vibration is in all three directions on the workpiece. For a point at the horizontal plane (between the shoulder/pin bottom and the workpiece), where the amplitude of vibration is ξ_0 and the velocity amplitude of the vibration is $\hat{v}$, we have,

$$\text{Longitudinal:}\quad \zeta_L=\omega r/\left(\hat{v}\cos\varpi\sin\theta\right) \tag{12}$$

$$\text{Transversal:}\quad \zeta_T=\omega r/\left(\hat{v}\cos\varpi\cos\theta\right) \tag{13}$$

where ω is the rotation speed, r is the length between the elemental and the tool axis, θ is the angle between the welding direction and the *r* radius vector direction.

When ζ_L and ζ_T are calculated from Eqs. (12) and (13), $\frac{\mu_L}{\mu_0}$ and $\frac{\mu_T}{\mu_0}$ is determined by

Eqs. (8) and (9). And $\frac{\mu_N}{\mu_0}$ is determined by the following equation,

$$\frac{\mu_n}{\mu_0}=\left(1-\frac{\alpha_N\xi\sin\varpi}{\tau}\right)\cdot\frac{\sqrt{\pi}}{\psi} \tag{14}$$

For a point at the contact interface between the pin side and the workpiece, where the amplitude of vibration is ξ and the velocity amplitude of the vibration is $\hat{v}$, we have

$$\text{Longitudinal:}\quad \zeta_L=\omega r/\left(\hat{v}\cos\varpi\sin\theta\right) \tag{15}$$

$$\text{Transvers:}\quad \zeta_T=\omega r/\left(\hat{v}\sin\varpi\right) \tag{16}$$

Then, $\frac{\mu_L}{\mu_0}$ and $\frac{\mu_T}{\mu_0}$ is determined by Eqs. (15) and (16). And $\frac{\mu_N}{\mu_0}$ is determined by the following equation,

$$\frac{\mu_N}{\mu_0}=\left(1-\frac{\alpha_N\xi\cos\varpi\cos\theta}{\tau}\right)\cdot\frac{\sqrt{\pi}}{\psi} \tag{17}$$

Taking into account the friction reduction effect from all three directions, the final friction coefficient after considering the ultrasonic friction reduction effect is the product of μ_L, μ_T, μ_N, and μ_0,

$$\mu_f=\frac{\mu_L}{\mu_0}\cdot\frac{\mu_T}{\mu_0}\cdot\frac{\mu_N}{\mu_0}\cdot\mu_0=\frac{\mu_L\cdot\mu_T\cdot\mu_N}{\mu_0^2} \tag{18}$$

And then, μ_f is used as the friction coefficient in the UVeFSW instead of μ_0 to calculate the velocity boundary and heat generation at the FSW tool-workpiece interface.

While for the other details for the UVeFSW CFD model, the control equations [17], boundary conditions [17,20], heat generation [17,20] of the FSW part, and the ultrasonic sound field [18] involved in the multi-field coupling model of Al-Mg dissimilar UVeFSW can refer to [17-20]. All the above were solved by employing the Ansys Fluent software. The volume fraction of each material was determined by the Volume of Fluid (VOF) method, and the physical parameters at each grid were weighted by the volume fractions of two materials inside the control element [17].

RESULTS AND DISCUSSION

ULTRASONIC FIELD OF AL/MG DISSIMILAR ALLOYS UVEFSW

Fig. 4 shows the acoustic energy distribution after the sound pressure field is stabilized in Al/Mg UVeFSW. From (a) to (c) are the acoustic energy distribution at x = 0 mm transverse cross-section, y = 0 mm longitudinal cross-section, and z = 1.5 mm horizontal

section, respectively. The AS, RS, LS, and TS in the figures are abbreviations of the advancing side, retreating side, leading side, and trailing side, respectively. Owing to the material flow and the different physical parameters between the two materials, the acoustic energy is distributed asymmetrically about the x-axis and y-axis.

The sonotrode was placed in front of the FSW tool and tilted forward, which conducts ultrasonic energy to the workpiece in front of the FSW tool, as shown in Fig. 4(b), the distribution law obtained from the longitudinal cross-section is similar to that of Al alloy UVeFSW [18]. While in the transverse cross-section (Fig. 4a), it is different from the Al alloy UVeFSW: (1) the acoustic energy is higher on the aluminum alloy (RS) than the Mg side (AS) due to the significantly different properties of aluminum alloy and magnesium alloy; (2) the acoustic energy distribution is no longer monotonically changes from one side to another but presents a pattern in the nugget zone, due to the complex material mixing in the weld nugget zone. While in the horizontal plane (Fig. 4c), on the one hand, the area with higher acoustic energy tends to extend to the tool pin as shown in the Al alloy UVeFSW [14], on the other hand, the high acoustic energy area tends to rotate around the FSW tool due to the influence of material distribution.

It is obvious that the sound energy field is distributed asymmetrically rather than symmetrically, because there are differences in physical parameters and plastic deformation between the two materials. The transmission of ultrasonic sound to the aluminum alloy side is more obvious, and the propagation of ultrasound in magnesium alloy is a little difficult. The density of magnesium alloy is smaller than that of aluminum alloy, and the sound speed in magnesium alloy is also smaller than that of aluminum alloy, resulting in a larger attenuation coefficient in magnesium alloy. The sound pressure on the magnesium alloy side is generally lower than that on the aluminum alloy side. According to the calculation process of the sound field, this is due to the low incoming sound pressure and large attenuation coefficient on the magnesium alloy side.

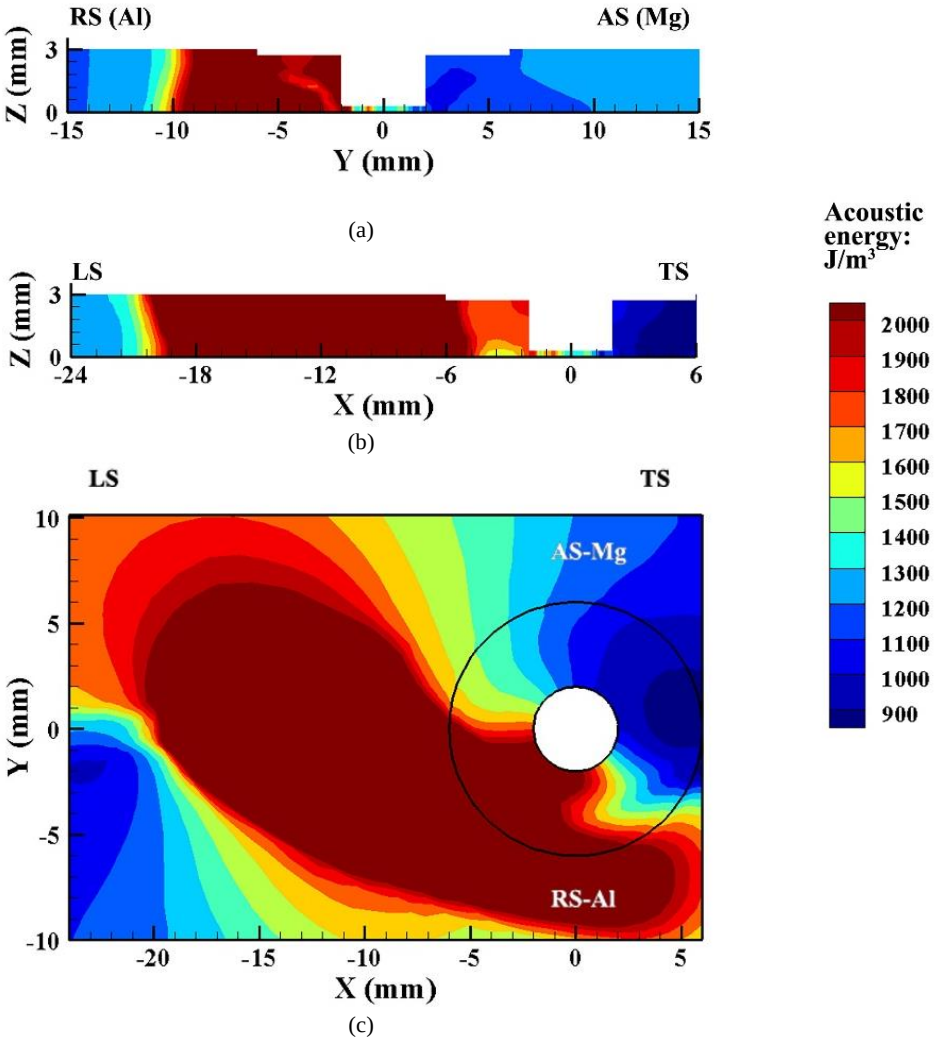

Fig. 4 The calculated acoustic energy density field at the (a) transverse cross-section, (b) longitudinal cross-section and (c) z = 1.5 mm horizontal plane

THE INFLUENCE OF ULTRASONIC VIBRATION ON FRICTION COEFFICIENT

Considering the UiFR effect, the friction coefficient distribution on the tool-workpiece interface in the Al/Mg dissimilar alloys UVeFSW model will be more complicated. Fig. 5 compares the distribution of the friction coefficient on the tool-workpiece contact interface with and without the UiFR effect.

Without UiFR, the friction coefficient gradually decreases with the increase of the distance away from the tool axis, because the slip ratio model and friction coefficient model proposed by Arora et al. [37] based on the rolling process, and a slight difference between AS and RS due to the dissimilar materials are placed on each side, as shown in Fig. 5(a).

After considering the UiFR effect, the friction coefficient near the tool axis is small and increases gradually with the increase of radial distance, which is similar to the case of 6061 UVeFSW [20]. Because the UiFR in the longitudinal direction plays a leading role [20], and according to Eq. (9), the smaller the ratio of material relative sliding speed to ultrasonic vibration speed is, the greater the UiFR effect will be. Based on that the amplitude of ultrasonic velocity is not much different at all parts of the FSW tool-workpiece contact interface, the closer the material is to the axis of the FSW tool, the smaller the relative sliding speed will be, and the smaller the ratio will be, the greater the UIFR effect will be.

However, in the case of Al-Mg UVeFSW, the UiFR effect is asymmetric due to the asymmetrical ultrasonic field, and finally, the friction coefficient presents a complex "deformed" butterfly shape, as shown in Fig. 5(b).

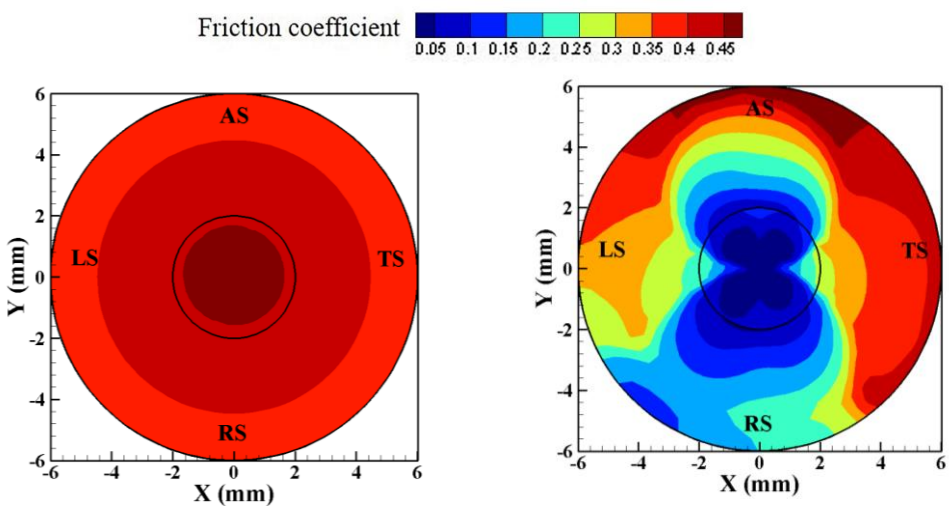

(a) Without UiFR

(b) With UiFR

Fig. 5 The distribution of friction coefficient on the tool-workpiece contact interfaces (vertical view)

THE EFFECT OF ULTRASONIC VIBRATION ON HEAT GENERATION AND TEMPERATURE

The heat generation of each part in FSW and UVeFSW models is compared in Table 1. It can be seen that after applying ultrasound, the sonotrode preheats the workpiece. Although the preheat effect will increase the temperature, the temperature around the

FSW tool will decrease due to the UiFR effect, and the viscous dissipation of the plastic deformation zone decreases with the viscosity.

Table 1 Comparison of the heat generation (W) of the contact interface in FSW/UVeFSW

	Shoulder	Shoulder side	Pin side	Pin bottom	Sonotrode	Viscous dissipation
FSW	315.069	67.159	45.465	22.119	0	94.64
UVeFSW	201.689	51.338	10.963	5.721	137.04	79.691

The friction coefficient distribution with the UiFR effect is very complex, making the heat flux distribution on the tool-workpiece interface becomes complex. The heat flux distribution of FSW/UVeFSW projected on the z = 0 mm horizontal plane is shown in Fig. 6. After applying ultrasonic, the distribution of friction coefficient is a "distorted" butterfly due to the UiFR effect, and the distribution of heat flux is distorted similarly as friction coefficient, but the deformation of the butterfly of heat flux is weakened by plastic heat generation. What's more, the heat flux is higher on AS than that on the RS after the ultrasonic application, because the degree of UiFR effect is different between the AS and RS.

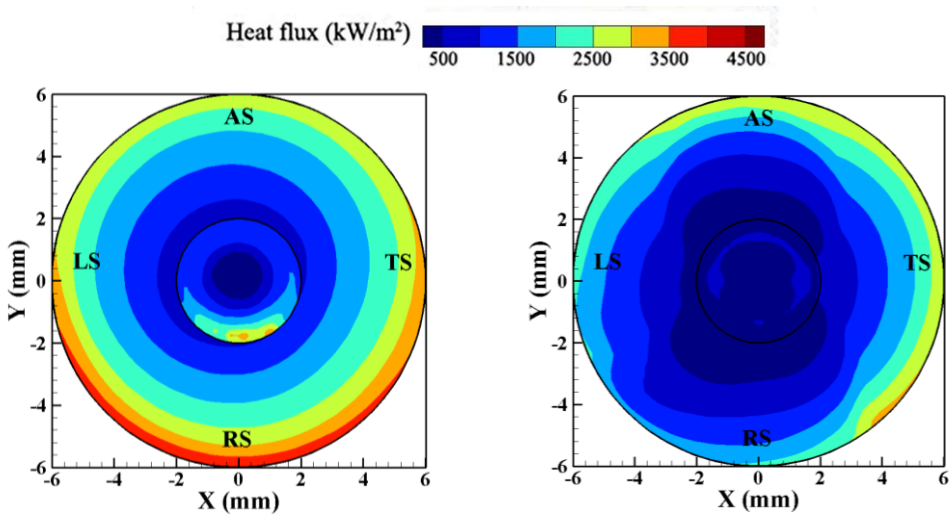

(a) FSW (b) UVeFSW

Fig. 6 The heat flux on the tool-workpiece contact interfaces in FSW/UVeFSW (vertical view).

Fig. 7 shows the temperature distribution on the top surface (including the shoulder). There is a small area in the sonotrode-workpiece interface where the temperature is higher due to the preheat of ultrasound.

For the tool-workpiece interface and its surroundings, after ultrasonic application, the highest temperature area around the tool pin disappears while the area of the sub-high temperature increases due to the coupling of the preheat and UiFR effects.

According to Fig. 5 and Fig. 6, the UiFR effect reduces the heat generation on the FSW tool-workpiece contact interface, so that the temperature of the part close to the contact interface will drop and the highest temperature area around the tool pin disappears.

However, due to the acoustic plastic effect of ultrasound, the softening effect of ultrasound is dominant in the area with a low strain rate, that is, the outer ring below the shoulder, and the flow stress will drop [20]. So that more areas will participate in the plastic deformation, resulting in viscous dissipation in more areas, so the sub-high temperature range will increase.

In addition, due to the preheating effect and the applied ultrasound to the leading side (LS), the high-temperature area shifts from the magnesium alloy (AS) to the area between AS and LS.

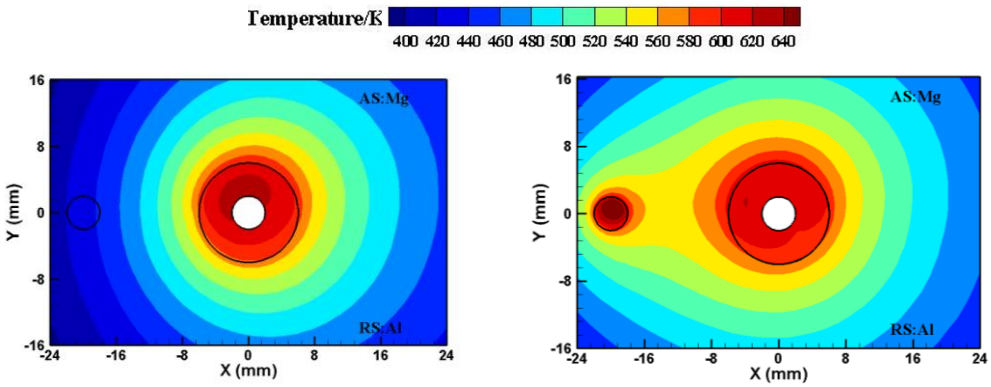

(a) FSW

(b) UVeFSW

Fig. 7 The calculated temperature on the top surface of the workpiece (including the contact surface of the shoulder)

THE EFFECT OF ULTRASONIC VIBRATION ON MATERIAL FLOW AND MIXING

Figs. 8 and 9 compare the macrograph of FSW and UVeFSW at different horizontal cross-sections with the corresponding calculation results, the right column is the experimental results, and the left column is the simulation results. In the simulation results, the boundary of the mixing zone is highlighted by the white dotted line.

After applying ultrasound, the width of the mixing zone becomes wider at the mid-depth plane (Fig. 8) and the plane of the pin bottom (Fig. 9), both in the experimental and calculated results, due to the acoustic plastic effect (soften and harden effects). The aluminum alloy goes deeper into AS (Fig. 8) also due to the acoustic plastic effect.

When we only studied the acoustic-plastic effect of ultrasound in FSW [20], we found that for the low level of the strain rate, the flow stress obtained by the constitutive equation considering ultrasonic hardening and softening is lower than that obtained by the constitutive equation only considering acoustic softening. When the strain rate is large enough, the flow stress calculated by the former is larger than that by the latter. The

acoustic softening and hardening effects dominate the conditions of high and low strain rates, respectively.

In the inner annular region near the pin side surface, the flow stress calculated by the constitutive equation considering ultrasonic hardening and softening is higher than that obtained by the constitutive equation only considering acoustic softening. But near the outer annular region, the flow stress by the former is lower than that by the latter.

It is easy to understand that at locations where the flow stress is reduced, the fluidity is improved, and it is easier to get rid of the rotating motion that follows the tool and to restore its horizontal flow in reverse to the welding direction. This means that if the flow stress in the region where the material flows through is reduced, the streamlines are not shifted to the rear AS.

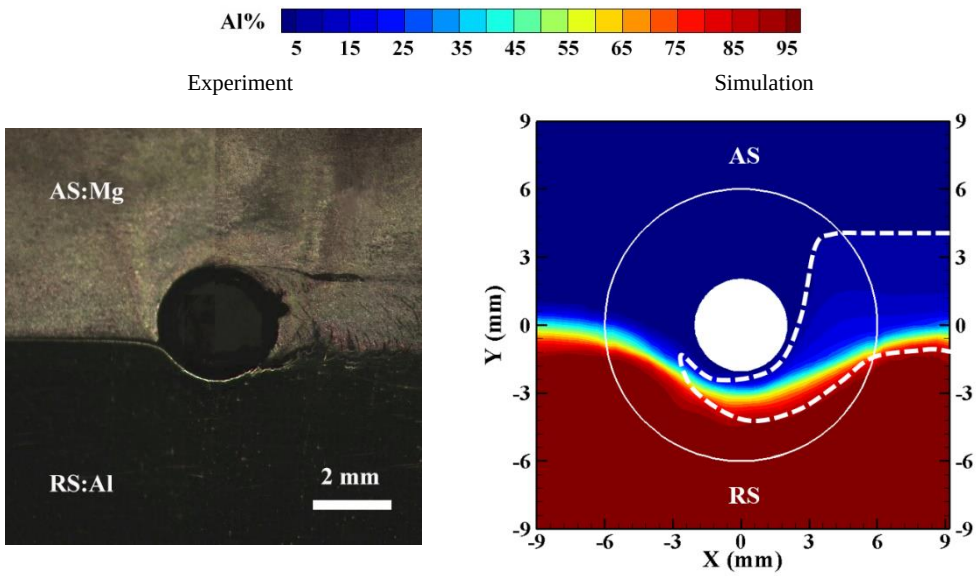

(a) FSW

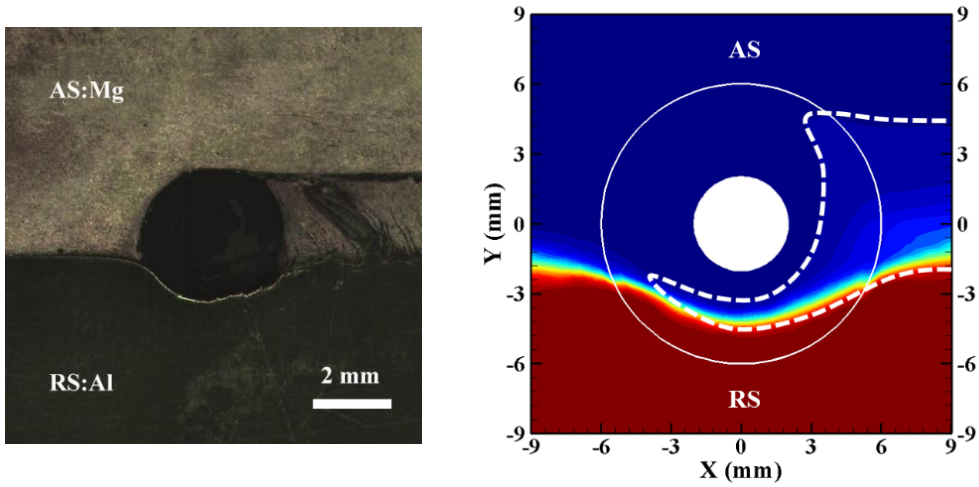

(b) UVeFSW

Fig. 8 The material distribution at mid-depth horizontal cross-sections

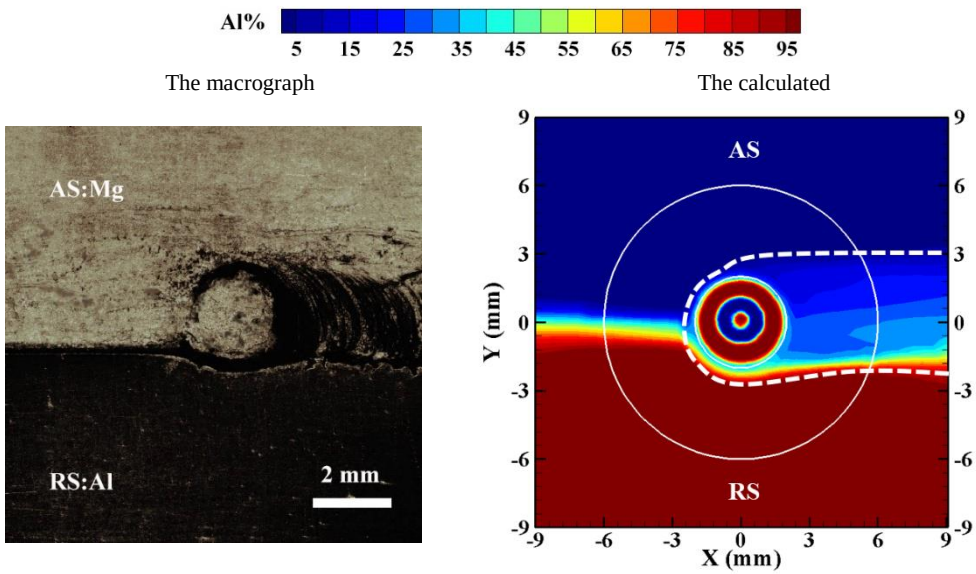

(a) FSW

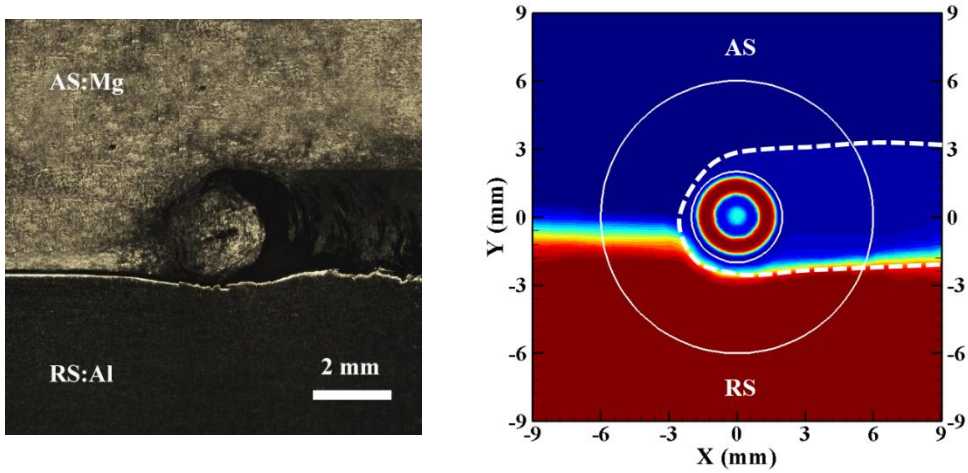

(b) UVeFSW

Fig. 9 The material distribution at the plane of pin bottom horizontal cross-sections

Considering the combined effect of hardening and softening of ultrasound, the flow stress in the outer region below the shoulder is reduced, and the material on the RS that flows through there is not offset toward the rear AS. However, at the inner region around the tool, the flow stress is not decreased, thus, the streamlines on the AS after bypassing the tool offset toward the rear AS. As the strain rate is gradually reduced from the inside to the outside of the regions covered by the FSW tool, the flow stress distribution of the inner and outer rings below the shoulder is different, which causes the flow lines flowing through different positions to be more biased toward the AS, while others are biased toward the RS. That means the combination of the two effects (acoustic softening and residual hardening) will lead to the widening of the mixed zone.

However, at the bottom of the tool pin or near the pin bottom surface, the strain rate is slightly higher. If only acoustic plasticity is considered, the softening of the material will be minimal at the inner ring below the shoulder, and the mixing will hardly be intensified. Therefore, it is difficult to explain this phenomenon just with the acoustic plastic effect. At the same time, the UiFR effect will also reduce the velocity boundary inputted as well as the material flow around the pin bottom. Therefore, the preheating effect is the main reason explaining the mixing intensification of the material around the pin bottom.

Additionally, at the plane of the pin bottom which did not show the acoustic hardening effect, the materials mixing just below the pin bottom is intensified, and the characteristics of ring-shaped aluminum outside and magnesium inside are weakened (Fig. 9), which is a consequence of the thermal effects.

CONCLUSIONS

In the Al/Mg UVeFSW model, the acoustic energy is stronger on the aluminum alloy side, the distribution of acoustic energy presents a pattern in the nugget zone, and the area

with high acoustic energy tends to extend to the tool pin and rotating around the FSW tool. Considering the ultrasonic vibration, the friction coefficient decreases. The distribution of the friction coefficient presents a "deformed" butterfly shape. With ultrasound, the heat generations at the tool-workpiece interface and the viscous dissipation are reduced. The heat flux at the tool-workpieces interface shows a less "deformed" butterfly-like than the friction coefficient. Comparing the material distributions with and without ultrasound at horizontal planes, the mechanism that ultrasonic vibration is beneficial to the mixing of dissimilar materials is clarified.

ACKNOWLEDGMENTS

The financial support from the National Natural Science Foundation of China (Grant No. 52035005) and the Humboldt Research Fellowship Programme for Postdoctoral Researchers are acknowledged.

References

[1] R. DHINGRA and S. DAS: 'Life cycle energy and environmental evaluation of downsized vs. lightweight material automotive engines', *J Clean Prod*, Vol. 85, pp. 347-358, 2014.

[2] B. L. FU, G. L. QIN, F. LI, X. M. MENG, J. Z. ZHANG and C. S. WU: 'Friction stir welding process of dissimilar metals of 6061-T6 aluminum alloy to AZ31B magnesium alloy', *J Mater Process Tech*, Vol. 218, pp. 38-47, 2015.

[3] L. H. SHAH, N. H. OTHMAN and A. GERLICH: 'Review of research progress on aluminum-magnesium dissimilar friction stir welding', *Sci Technol Weld Joi*, Vol. 23, pp. 256-270, 2018.

[4] L. E. MURR: 'A review of FSW research on dissimilar metal and alloy systems', *J Mater Eng Perform*, Vol. 19, pp. 1071-1089, 2010.

[5] A. ESMAEILI, C. SBARUFATTI and A. M. S. HAMOUDA: 'Characteristics of intermetallic compounds in dissimilar friction stir welding: a review', *Metallography Microstructure and Analysis*, Vol. 8, pp. 445-461, 2019.

[6] S. KUMAR, C. S. WU and S. GAO: 'Process parametric dependency of axial downward force and macro-and microstructural morphologies in ultrasonically assisted friction stir welding of Al/ Mg alloys', *Metall Mater Trans A*, Vol. 51, pp. 2863-2881, 2020.

[7] M. THOMÄ, G. WAGNER, B. STRAß, C. CONRAD, B. WOLTER, S. BENFER and W. FÜRBETH: 'Realization of ultrasound enhanced friction stir welded Al/Mg and Al/Steel-joints: process and robustness, mechanical and corrosion properties', *Minerals Metals & Materials Series*, Friction Stir Welding and Processing IX, Part V, pp. 179-194, 2017.

[8] B. STRASS, G. WAGNER, C. CONRAD, B. WOLTER, S. BENFER and W. FÜBETH: 'Realization of Al/Mg-Hybrid-Joints by ultrasound supported friction stir welding-mechanical properties, microstructure and corrosion behavior', *Minerals Metals & Materials Series*, Vol. 966, pp. 521-535, 2017.

[9] M. THOMÄ, G. WAGNER, B. STRAß, C. CONRAD, B. WOLTER, S. BENFER and W. FÜRBETH: 'Recent developments for ultrasonic-assisted friction stir welding: joining, testing, corrosion-an overview', *IOP Conf Ser Mater Sci Eng*, Vol. 118, No. 1, pp. 012014, 2016.

[10] S. BENFER, B. STRASS, G. WAGNER and W. FÜBETH: 'Manufacturing and corrosion properties of ultrasound supported friction stir welded Al/Mg-hybrid joints', *Surf Interface Anal*, Vol. 48, No. 8, pp. 850-859, 2016.

[11] S. D. JI, X. C. MENG, Z. L. LIU, R. F. HUANG and Z. W. LI: 'Dissimilar friction stir welding of 6061 aluminum alloy and AZ31 magnesium alloy assisted with ultrasonic', *Mater Lett*, Vol. 201, pp. 173-176, 2017.
[12] X. C. MENG, Y. Y. JIN, S. D. JI and D. J. YAN: 'Improving friction stir weldability of Al/Mg alloys via ultrasonically diminishing pin adhesion', *J Mater Sci Technol*, Vol. 34, pp. 1817-1822, 2018.
[13] Z.L. LIU, X. C. MENG, S. D. JI, Z. W. LI and L. WANG: 'Improving tensile properties of Al/Mg joint by smashing intermetallic compounds via ultrasonic-assisted stationary shoulder friction stir welding', *J Manuf Process*, Vol. 31, pp. 552-559, 2018.
[14] X. Q. LV, C. S. WU, C. L. YANG and G. K. PADHY: 'Weld microstructure and mechanical properties in ultrasonic enhanced friction stir welding of Al alloy to Mg alloy', *J Mater Process Tech*, Vol. 254, pp. 145-157, 2018.
[15] A. K. SINGH, P. SAHLOT, M. PALIWAL and A. ARORA: 'Heat transfer modeling of dissimilar FSW of Al 6061/AZ31 using experimentally measured thermo-physical properties', *Int J Adv Manuf Tech*, Vol. 105, pp. 771-783, 2019.
[6] J. Y. LIM and J. H. LEE: 'Development of a coupled Eulerian-Lagrangian finite element model for dissimilar friction stir welding', *Journal of the Korea Academia-Industrial cooperation Society*, Vol. 20, pp. 7-13, 2019.
[17] C. L. YANG, C. S. WU and X. Q. LV: 'Numerical analysis of mass transfer and material mixing in friction stir welding of aluminum/magnesium alloys', *J Manuf Process*, Vol. 32, pp. 380-394, 2018.
[18] L. SHI, C. S. WU, S. GAO and G. K. PADHY: 'Numerical simulation of ultrasonic field and its acoustoplastic influence on friction stir welding', *Mater Design*, Vol. 104, pp. 102-115, 2016.
[19] C. L. YANG and C. S. WU: 'Constitutive equation with residual hardening effect for modeling the ultrasonic vibration enhanced friction stir welding process', *Sci Technol Weld Joi*, Vol. 24, pp. 695-705, 2019.
[20] C. L. YANG, C. S. WU and L. SHI: 'Analysis of friction reduction effect due to ultrasonic vibration exerted in friction stir welding', *J Manuf Process*, Vol. 35, pp. 118-126, 2018.
[21] S. ELANGOVAN, S. SEMEER and K. PRAKASAN: 'Temperature and stress distribution in ultrasonic metal welding-an FEA-based study', *J Mater Process Tech*, Vol. 209, No.3, pp. 1143-1150, 2009.
[22] B. LANGENECKER: 'Effects of ultrasound on deformation characteristics of metals', *IEEE Transactions on Sonics and Ultrasonics*, Vol. 13, pp. 1-8, 1966.
[23] A. S. KRAUSZ and K. KRAUSZ: 'Unified constitutive laws of plastic deformation', *San Diego: Academic Press*, 1996.
[24] Y. Y. DONG, C. S. ZHANG, X. LU, C. X. WANG and G. Q. ZHAO: 'Constitutive equations and flow behavior of an as-extruded AZ31 magnesium alloy under large strain condition', *J Mater Eng Perform*, Vol. 25, pp. 2267-2281, 2016.
[25] Z. Z. YU, W. ZHANG, H. CHOO and Z. L. FENG: 'Transient heat and material flow modeling of friction stir processing of magnesium alloy using threaded tool', *Metall Mater Trans*, Vol. 43A, No. 2, pp. 724-737, 2016.
[26] X. C. LIU, C. S. WU and K. P. GIRISH: 'Characterization of plastic deformation and material flow in ultrasonic vibration enhanced friction stir welding', *Scripta Mater*, Vol. 102, pp. 95-98, 2015.
[27] H. MECKING and U. F. KOCKS: 'Kinetics of flow and strain-hardening', *Acta Metall*, Vol. 29, No. 11, pp. 1865-1875, 1981.
[28] U. F. KOCKS: 'Laws for work-hardening and low-temperature creep', *J Eng Mater-T*, Vol. 98, No. 1, pp. 76-85, 1976.
[29] J. H. M. THORNLEY, J. J. SHEPHERD and J. FRANCE: 'An open-ended logistic-based growth function: Analytical solutions and the power-law logistic mode', *Ecologistic Modelling*, Vol. 204, pp. 531-534, 2007.

[30] A. TSOULARIS and J. WALLACE: 'Analysis of logistic growth models', *Mathematical Biosciences*, Vol. 179, pp. 21-55, 2002.
[31] B. GALLAGHER: 'Peak oil analyzed with a logistic function and idealized Hubbert curve', *Energy Policy*, Vol. 39, No. 2, pp. 790-802, 2011.
[32] H. H. CHO, S. T. HONG, J. H. ROH, H. S. CHOI, S. H. KANG, R. J. STEEL and H. N. HAN: 'Three dimensional numerical and experimental investigation on friction stir welding processes of ferritic stainless steel', *Acta Mater*, Vol. 61, pp. 2649-2661, 2013.
[33] P. GUTOWSKI and M. LEUS: 'The effect of longitudinal tangential vibrations on friction and driving forces in sliding motion', *Tribol Int*, Vol. 55, pp. 108-118, 2012.
[34] H. STORCK, W. LITTMANN, J. WALLASCHEK and M. MRACEK: 'The effect of friction reduction in presence of ultrasonic vibrations and its relevance to traveling wave ultrasonic motors', *Ultrasonics*, Vol. 40, pp. 379-383, 2002.
[35] W. LITTMANN, H. STORCK and J. WALLASCHEK: 'Sliding friction in the presence of ultrasonic oscillations: superposition of longitudinal oscillations', *Arch Appl Mech*, Vol. 71, No. 8, pp. 549-554, 2001.
[36] J. A. GREENWOOD and J. B. P. WILLIAMSON: 'Contact of nominally flat surfaces', *Proceedings of the ROYAL Society of London Series A-Mathematical and Physical Sciences* Vol. 295, No. 1442, pp. 300-319, 1996.
[37] A. ARORA, A. DE, T. DEBROY: 'Toward optimum friction stir welding tool shoulder diameter', *Scripta Mater*, Vol. 64, pp. 9-12, 2011.